Accurate and Efficient Numerical Method for the Analysis of Multimode Waveguide Discontinuities

Philippe Pannier, Lhoussain Kadri, Christophe Seguinot, Patrick Kennis, and Fabrice Huret

***Abstract*—This paper presents an original approach to analyze multimode waveguide discontinuities. The generalized scattering parameters are determined by a matrix pencil moment method associated with efficient numerically multimode matched loads placed at each physical port of the discontinuities. The analysis of both microstrip-coupled lines and coplanar lines asymmetric discontinuities is presented and successfully compared to experiments and available published results.**

***Index Terms*—Discontinuities, multimode waveguides, numerical technique, scattering parameters.**

I. Introduction

With the increasing complexity of microwave and millimeter-wave integrated circuits, passive component modeling becomes more and more important in accurately determining the performances of the designed circuits, especially junction discontinuities. Today, three-dimensional (3-D) passive circuit structures are formed to implement highly dense and more functional monolithic microwave integrated circuits (MMIC's). The 3-D MMIC technology effectively reduces the circuit area and allows to significantly multiply the integration level [1], [2]. This further increases coupling and makes it awkward to use many of the standard junctions. Consequently, higher operating frequency and higher performance requirements have made some of models, based on a quasi-static assumption, not accurate enough. Fully electromagnetic models are now often required in order to include effects such as dispersion, radiation, and coupling.

From another point-of-view, the integration levels of the ultra-compact MMIC's require the characterization and the modeling of multiple line interconnections. Consequently, a multiple-mode behavior must be considered for many topologies. As example, a coupled microstrip line supports two quasi-TEM modes [3]. A parasitic mode coupling can then occur when an asymmetric discontinuity appears in the circuit. In order to improve the isolation characteristics in ultra-compact MMIC's, in [1], two microstrip lines have been shielded employing a vertical metal wall. However, the achievement of the topologies used in order to suppress the mode coupling and mode conversion can only be appreciated if we consider that multiple modes are propagated by the waveguide.

Today, planar MMIC's are realized more and more by using the coplanar waveguide (CPW) [4]. The transmission-line configuration in coplanar MMIC's consists of three or four conductor-backed CPW nonconnected electrodes and, therefore, two or three quasi-TEM modes are supported by this topology. The coplanar and slot-line modes are the fundamental modes of the CPW. A parallel-plate mode can also occur in conductor-backed coplanar transmission lines. In conductor-backed coplanar MMIC's, power can be transferred from the coplanar mode to the parallel-plate one by leakage effect and coupling between the modes at transmission-line discontinuities [5]. In [6], conductor-backed CPW-to-microstrip transition is studied and the mode conversion between the coplanar mode and parasitic parallel-plate mode is presented. In [7], the coupling between the fundamental CPW mode and undesired parallel-plate mode at coplanar open and short circuits is analyzed by means of a finite-difference method. The excitation of the slotline mode is also a main problem if asymmetric discontinuities, like bends, are built [8], [9]. Air bridges are commonly used to suppress the slotline mode [10], [11]. The use of top and/or bottom ground-plane shields has been also employed to suppress this parasitic mode [12]. Recently, a full-wave algorithm has been proposed to analyze the mode conversion in a CPW right-angle bend [9]. Based on a multiple-pencil integral-equation (MPIE) formulation, this algorithm solves the integral equation by a moment method using finite-element rooftop basis functions. Given the magnetic current distribution on the apertures, the matrix pencil approach is them employed to do the deembedding procedure and extract the scattering parameters of all the modes.

In this procedure, open- and short-circuited terminations are generally involved. The scattering parameters of devices are then deduced from the calculated densities of surface currents flowing on the structure. They require a nondirect calculation involving deembedding procedures in order to compensate for the effect of opens or shorts. Several simulations are needed to compute the whole scattering-parameter matrix. Moreover, with the operating frequency increase, high reflection coefficients are expected to spoil the accuracy of the calculations.

Manuscript received June 16, 1999.

P. Pannier is with the Laboratoire de Modélization et de Microélectronique de Marseille, ICF, IMT, 13451 Marseille, France.

L. Kadri, C. Seguinot, and P. Kennis are with the Institut d'Electronique et de Microélectronique du Nord, UMR CNRS 9929, Domaine Scientifique et Universitaire de Villeneuve d'Ascq, 59652 Villeneuve d'Ascq, France.

F. Huret is with the Institut d'Electronique et de Microélectronique du Nord, U.M.R. CNRS 9929 Domaine Scientifique et Universitaire de Villeneuve d'Ascq, 59652 Villeneuve d'Ascq, France, and is also with the Laboratoire d'Etude des Matériaux et des Composants pour l'Electronique, Université du Littoral–Côte d'Opale, IUT du Littoral, 1 62228 Calais, France (e-mail: Fabrice.Huret@IEMN.Univ-Lille1.fr).

Publisher Item Identifier S 0018-9480(00)00843-7.

This paper presents a full-wave analysis of multiple-mode waveguide discontinuities using a spectral-domain approach. Based on an electric (or magnetic)-field integral-equation formulation, the electric (or magnetic)-current distribution on the device is solved by the well-known Galerkin's moment method [13], [14]. The generalized scattering parameters are numerically measured with the help of an efficient numerically multimode matched loads (NMML's) placed at each physical port of the discontinuities. With that in mind, the matrix pencil technique [15]–[17] is used to decompose the currents of all the guided waves, along the terminating lines, into only forward-traveling waves and the currents along the feeding lines into forward- and backward-traveling waves, yielding scattering parameters of the device without the deembedding procedure.

Formulation and theoretical aspects are presented in Section II. When the continuity of the electric field is enforced at the conductor's surface, the electromagnetic-field problem can be described by an electric-field integral equation (EFIE) for the surface current distribution. Moreover, when slot and coplanar lines are taking into account, the equivalence principle allows us to describe these structures with the help of magnetic current in the slots. The continuity condition of the tangential magnetic field leads to a magnetic-field integral equation [18], [19]. The NMML may be applied in the case of magnetic-current-defined structures (CPW) as well as in the case of structures defined with the presence of electric-current densities (multiple microstrip coupled lines). In order to explain this original numerical technique, we propose to apply it in the mathematical framework of the EFIE resolution associated with a three-conductor's waveguide.

In Section III, numerical results and validating examples are presented. In this case, both microstrip coupled-line and coplanar-line asymmetric discontinuities are simulated. A multimode thru-reflection line (TRL) calibration is also used to derive experimental multimode S-parameters [20]. Our measurements and full-wave results are in excellent agreement. The results are also in agreement with published data [9]. Finally, brief conclusions are drawn in Section IV.

II. Theory

A. EFIE Formulation

Since the method of moments is well known, it is only discussed briefly in order to set the notation and to note some salient points.

Fig. 1 shows the basic studied multiple-mode device. A microstrip line is connected to a coupled microstrip line. The asymmetry of this device implies that the two fundamental quasi-TEM modes will be propagated in the outcoming waveguide. We have to notice that the ground plane and dielectric substrate extend to infinity in the x- and y-directions. The conductors are assumed to be perfect and of zero thickness.

The electromagnetic-field problem associated with the structure shown in Fig. 1 is described by an EFIE for the surface current distribution $\vec{J}(x, y)$. This leads to

$$\iint_s \left(\vec{E}_d + \vec{E}_{\text{exc}}\right) \cdot \vec{J}_d.dx.dy = 0 \tag{1}$$

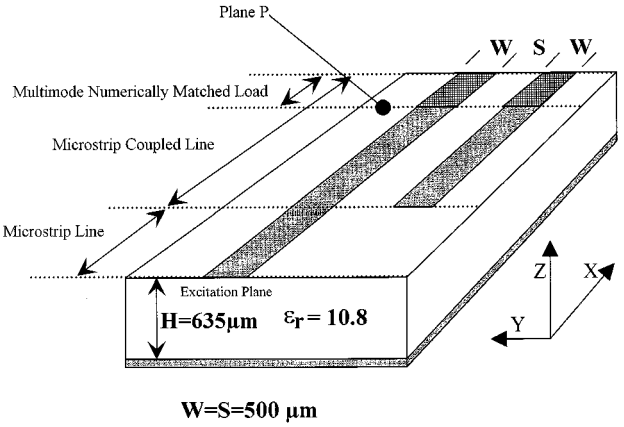

Fig. 1. Multimode structure.

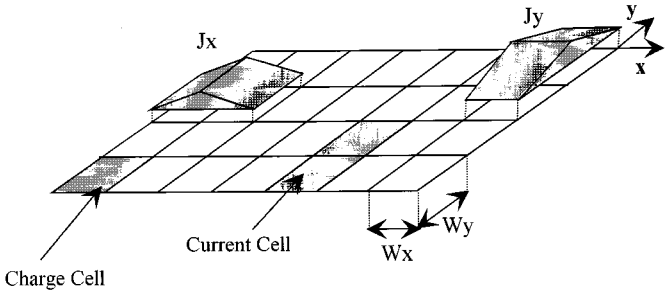

Fig. 2. Basis functions employed on the segmented microstrip coupled line.

where $\vec{E}_d$ is the diffracted electric field due to the surface current densities $\vec{J}_d$ and $\vec{E}_{exc}$ is the impressed electric field due to the excitation mechanism. The previous integral equation is expressed in the Fourier domain and solved using the method of moments where electric-current densities are expanded in terms of rooftop basis functions. These basis functions are depicted in Fig. 2. The Galerkin's method is then applied to project the integral equation onto a system of linear equations in the form

$$\begin{bmatrix} Z_{ij} \end{bmatrix} \cdot \begin{bmatrix} I_1 \\ I_2 \\ \\ I_N \end{bmatrix} = \begin{bmatrix} V \end{bmatrix} \tag{2}$$

where Z_{ij} is the reaction term between the ith test function and the jth basis function and may be written as

$$Z_{ij} = \int_{-\infty}^{+\infty} \int_{-\infty}^{+\infty} \tilde{G}(\alpha, \beta) \cdot \tilde{J}_j(\alpha, \beta) \cdot \tilde{J}_i^*(\alpha, \beta) \cdot d\alpha \cdot d\beta \tag{3}$$

where $\tilde{J}_i(\alpha, \beta)$ and $\tilde{J}_j(\alpha, \beta)$ are the Fourier transform expressions of subsectional test function i and basis function j with respect to Fourier-transform variables α and β and $\tilde{G}(\alpha, \beta)$ is the appropriate dyadical Green's function for the electric field. Weighting coefficients $I_1, I_2, \cdots, I_N$ constitute the unknowns of the problem. The excitation is modeled by ideal x-directed voltage sources located at specific node points, resulting in an excitation vector $[V]$, which has zeros everywhere, except at the positions of these voltage sources. These excitations are delta gap voltage generators [21], [22].

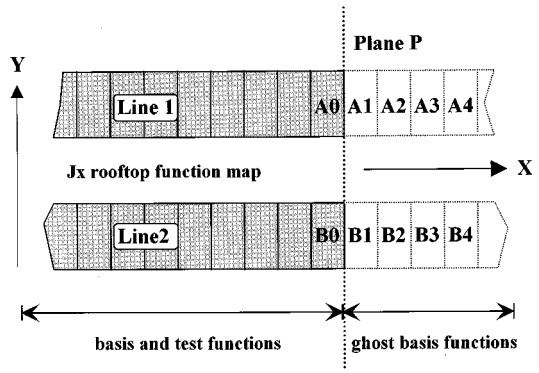

Fig. 3. Current density rooftop function map for the structure shown in Fig. 1 with a one-cell division along the strip width.

B. NMML Formulation

1) Basic Principles of the NMML: In this section, we exhibit the modeling of the NMML in the particular case of the coupled microstrip line shown in Fig. 1, matched at one extremity in the reference plane P. Throughout this section, we consider that the waves propagate in the X-direction.

For that device, we define over a grid the basis and test functions both for Jx and Jy current densities. In order to simplify the formulation presentation, a simpler division using only one cell along the strip width is first employed. Since rooftop functions are overlapped over two cells, only longitudinal component Jx of the current density is taken into account, as shown in Fig. 3.

Assuming that only the two fundamental modes propagate on the lossless microstrip coupled line, the longitudinal current distributions can be seen as the sum of both two incidents and reflected currents. On the lines, it can be expressed as

$$\vec{J}(x,y) = \vec{a}_e(y)\cdot e^{-2\pi j(x/\lambda g_e)} + \vec{b}_e(y)\cdot e^{2\pi j(x/\lambda g_e)} + \vec{a}_o(y)\cdot e^{-2\pi j(x/\lambda g_o)} + \vec{b}_o(y)\cdot e^{2\pi j(x/\lambda g_o)} \quad (4)$$

where $\vec{a}_e$ and $\vec{a}_o$ are the incident currents of, respectively, even and odd modes, $\vec{b}_e$ and $\vec{b}_o$ are related to the reflected currents, and λg_e and λg_o are the guided wavelengths of the two different modes. The NMML can then be simulated by imposing the cancellation of the reflected waves. This absorbing condition is obtained by forcing the current density at the end of the lines to belong to a traveling wave [23]–[25]. The most important difficulty lies in fact that multiple modes propagate in the lines and the total current density results in a superposition of different current densities with a different wavenumber.

2) Moment-Method Resolution: As shown in Figs. 1 and 3, P is the reference plane where the NMML connects. The last Jx basis functions before the matched load are denoted $A0$ in line 1, $B0$ in line 2, associated with the weighting coefficients I_{A0} and I_{B0}. The matched load is modeled by forcing the current density, behind reference plane P, to belong to a traveling wave. With that in mind, rooftop Jx basis functions are added to the lines and have unknown weighting coefficients $I_{Ai}, I_{Bi} (i = 1, 2, 3, \cdots)$. The longitudinal current density amplitude flowing over an infinite line has the following expression:

$$\vec{J}x(x) = \vec{a}_e\cdot e^{-2\pi j(x/\lambda g_e)} + \vec{a}_o\cdot e^{-2\pi j(x/\lambda g_o)} \quad (5)$$

where $\vec{a}_e$ and $\vec{a}_o$ are related to the even and odd modes.

For monomode circuits, the unknown weighting coefficients of added basis functions might be related to each other with a simple recurrent relation [23]. For multimode circuits, several current densities with a different amplitude and guided wavelength are superimposed. Thus, the NMML must be built with more complicated coupled recurrent relations where all mode contributions are identified. In the particular case of a coupled microstrip line, two coupled recurrent relations are need. This formulation is now presented.

I_{A0} can be expressed as

$$I_{A0} = \left(\frac{I_{B0}+I_{A0}}{2}\right) - \left(\frac{I_{B0}-I_{A0}}{2}\right). \quad (6)$$

I_{B0} can be expressed as

$$I_{B0} = \left(\frac{I_{B0}+I_{A0}}{2}\right) + \left(\frac{I_{B0}-I_{A0}}{2}\right). \quad (7)$$

According to the symmetry properties $((I_{B0}+I_{A0})/2)$ and $((I_{B0}-I_{A0})/2)$ are, respectively, the even- and odd-mode current density amplitudes.

Equation (5) gives

$$I_{B1} = \left(\frac{I_{B0}+I_{A0}}{2}\right)\cdot e^{-2\pi j(Wx/\lambda g_e)} + \left(\frac{I_{B0}-I_{A0}}{2}\right)\cdot e^{-2\pi j(Wx/\lambda g_o)} \quad (8)$$

$$I_{A1} = \left(\frac{I_{B0}+I_{A0}}{2}\right)\cdot e^{-2\pi j(Wx/\lambda g_e)} - \left(\frac{I_{B0}-I_{A0}}{2}\right)\cdot e^{-2\pi j(Wx/\lambda g_o)} \quad (9)$$

where Wx is the length of a unit rectangular cell with respect to the x-direction.

After simplifications, (8) and (9) become

$$I_{B1} = \frac{I_{B0}}{2}\cdot\left(e^{-2\pi j(Wx/\lambda g_e)} + e^{-2\pi j(Wx/\lambda g_o)}\right) + \frac{I_{A0}}{2}\cdot\left(e^{-2\pi j(Wx/\lambda g_e)} - e^{-2\pi j(Wx/\lambda g_o)}\right) \quad (10)$$

$$I_{A1} = \frac{I_{B0}}{2}\cdot\left(e^{-2\pi j(Wx/\lambda g_e)} - e^{-2\pi j(Wx/\lambda g_o)}\right) + \frac{I_{A0}}{2}\cdot\left(e^{-2\pi j(Wx/\lambda g_e)} + e^{-2\pi j(Wx/\lambda g_o)}\right). \quad (11)$$

In a next stage, the weighting coefficients I_{A2} and I_{B2} can be expressed as

$$I_{B2} = \left(\frac{I_{B1}+I_{A1}}{2}\right)\cdot e^{-2\pi j(Wx/\lambda g_e)} + \left(\frac{I_{B1}-I_{A1}}{2}\right)\cdot e^{-2\pi j(Wx/\lambda g_o)} \quad (12)$$

$$I_{A2} = \left(\frac{I_{B1}+I_{A1}}{2}\right)\cdot e^{-2\pi j(Wx/\lambda g_e)} - \left(\frac{I_{B1}-I_{A1}}{2}\right)\cdot e^{-2\pi j(Wx/\lambda g_o)}. \quad (13)$$

We then put (10)) and (11) in place of I_{B1} and I_{A1}. As an example, (12) leads to

$$\begin{aligned} I_{B2} = &\left[\frac{I_{B0}}{4}\cdot\left(e^{-2\pi j(Wx/\lambda g_e)}+e^{-2\pi j(Wx/\lambda g_o)}\right)\right.\\ &+\frac{I_{A0}}{4}\cdot\left(e^{-2\pi j(Wx/\lambda g_e)}-e^{-2\pi j(Wx/\lambda g_o)}\right)\\ &+\frac{I_{B0}}{4}\cdot\left(e^{-2\pi j(Wx/\lambda g_e)}-e^{-2\pi j(Wx/\lambda g_o)}\right)\\ &\left.+\frac{I_{A0}}{4}\cdot\left(e^{-2\pi j(Wx/\lambda g_e)}+e^{-2\pi j(Wx/\lambda g_o)}\right)\right]\\ &\cdot e^{-2\pi j(Wx/\lambda g_e)}\\ &+\left[\frac{I_{B0}}{4}\cdot\left(e^{-2\pi j(Wx/\lambda g_e)}+e^{-2\pi j(Wx/\lambda g_o)}\right)\right.\\ &+\frac{I_{A0}}{4}\cdot\left(e^{-2\pi j(Wx/\lambda g_e)}-e^{-2\pi j(Wx/\lambda g_o)}\right)\\ &-\frac{I_{B0}}{4}\cdot\left(e^{-2\pi j(Wx/\lambda g_e)}-e^{-2\pi j(Wx/\lambda g_o)}\right)\\ &\left.-\frac{I_{A0}}{4}\cdot\left(e^{-2\pi j(Wx/\lambda g_e)}+e^{-2\pi j(Wx/\lambda g_o)}\right)\right]\\ &\cdot e^{-2\pi j(Wx/\lambda g_o)}. \end{aligned} \tag{14}$$

After simplification, this leads to

$$\begin{aligned} I_{B2} = &\frac{I_{B0}}{2}\cdot\left(e^{-4\pi j(Wx/\lambda g_e)}+e^{-4\pi j(Wx/\lambda g_o)}\right)\\ &+\frac{I_{A0}}{2}\cdot\left(e^{-4\pi j(Wx/\lambda g_e)}-e^{-4\pi j(Wx/\lambda g_o)}\right). \end{aligned} \tag{15}$$

I_{A2} can be expressed in the same way as

$$\begin{aligned} I_{A2} = &\frac{I_{B0}}{2}\cdot\left(e^{-4\pi j(Wx/\lambda g_e)}-e^{-4\pi j(Wx/\lambda g_o)}\right)\\ &+\frac{I_{A0}}{2}\cdot\left(e^{-4\pi j(Wx/\lambda g_e)}+e^{-4\pi(Wx/\lambda g_o)}\right). \end{aligned} \tag{16}$$

According to the (15) and (16), weighting coefficients of added basis functions Ai and Bi may be related to each other with two coupled recurrent relations as

$$\begin{aligned} I_{Bn} = &\frac{I_{B0}}{2}\cdot\left(e^{-2n\pi j(Wx/\lambda g_e)}+e^{-2n\pi j(Wx/\lambda g_o)}\right)\\ &+\frac{I_{A0}}{2}\cdot\left(e^{-2n\pi j(Wx/\lambda g_e)}-e^{-2n\pi j(Wx/\lambda g_o)}\right) \end{aligned} \tag{17}$$

$$\begin{aligned} I_{An} = &\frac{I_{B0}}{2}\cdot\left(e^{-2n\pi j(Wx/\lambda g_e)}-e^{-2n\pi j(Wx/\lambda g_o)}\right)\\ &+\frac{I_{A0}}{2}\cdot\left(e^{-2n\pi j(Wx/\lambda g_e)}+e^{-2n\pi j(Wx/\lambda g_o)}\right). \end{aligned} \tag{18}$$

Under this condition, the weighting coefficients of the added basis functions are related to the I_{A0}, I_{B0} unknown coefficients, thus, test functions over the matched load are useless. Added basis functions on the matched load are, for that reason, called "ghost basis functions" [23]. We have to notice that with the previous relations (17) and (18), the final matrix system size does not inflate with the presence of NMML. The final matrix system of the problem is, with regard to the one without matched loads, changed by the accounting of the electric field diffracted by ghost basis functions on an NMML. For each test function i lying on the studied structure, the reaction terms related to the unknown weighting coefficients of the last basis functions I_{A0} and I_{B0} are changed in agreement with (17) and (18), and the matrix system to solve becomes

$$\begin{array}{c} \\ 1 \\ \\ \\ \\ i \\ \\ \\ \end{array}\begin{array}{c} \begin{array}{cccccc} 1 & & A0 & & B0 & \end{array} \\ \begin{pmatrix} Z_{1,1} & & \vdots & & \vdots & \\ & & \vdots & & \vdots & \\ & & \vdots & & \vdots & \\ \cdots & \cdots & Z'_{i,A0} & \cdots & Z'_{i,B0} & \cdots \\ & & \vdots & & \vdots & \\ & & \vdots & & \vdots & \\ & & \vdots & & \vdots & \end{pmatrix} \end{array} \cdot \begin{pmatrix} I_1 \\ \vdots \\ I_{A0} \\ \vdots \\ I_{B0} \\ \vdots \end{pmatrix} = \begin{pmatrix} V_1 \\ V2 \\ \vdots \\ \vdots \\ \vdots \\ \vdots \end{pmatrix} \tag{19}$$

with

$$\begin{aligned} Z'_{i,A_0} = &Z_{i,A0}\\ &+\frac{1}{2}\left[Z_{i,A1}\cdot\left(e^{-2\pi j(Wx/\lambda g_e)}+e^{-2\pi j(Wx/\lambda g_o)}\right)\right.\\ &\left.+Z_{i,B1}\cdot\left(e^{-2\pi j(Wx/\lambda g_e)}-e^{-2\pi j(Wx/\lambda g_o)}\right)\right]\\ &+\frac{1}{2}\left[Z_{i,A2}\cdot\left(e^{-4\pi j(Wx/\lambda g_e)}+e^{-4\pi j(Wx/\lambda g_o)}\right)\right.\\ &\left.+Z_{i,B2}\cdot\left(e^{-4\pi j(Wx/\lambda g_e)}-e^{-4\pi j(Wx/\lambda g_o)}\right)\right]\\ &+\cdots\cdots\cdots \end{aligned} \tag{20}$$

$$\begin{aligned} Z'_{i,B0} = &Z_{i,B0}\\ &+\frac{1}{2}\left[Z_{i,B1}\cdot\left(e^{-2\pi j(Wx/\lambda g_e)}+e^{-2\pi j(Wx/\lambda g_o)}\right)\right.\\ &\left.+Z_{i,A1}\cdot\left(e^{-2\pi j(Wx/\lambda g_e)}-e^{-2\pi j(Wx/\lambda g_o)}\right)\right]\\ &+\frac{1}{2}\left[Z_{i,B2}\cdot\left(e^{-4\pi j(Wx/\lambda g_e)}+e^{-4\pi j(Wx/\lambda g_o)}\right)\right.\\ &\left.+Z_{i,A2}\cdot\left(e^{-4\pi j(Wx/\lambda g_e)}-e^{-4\pi j(Wx/\lambda g_o)}\right)\right]\\ &+\cdots\cdots\cdots. \end{aligned} \tag{21}$$

3) Generalization: In many applications, a simpler division using only one cell along the width of the lines is not sufficient to achieve convergent extracted modal amplitudes, particularly in millimeter frequency range. A more detailed division will then be necessary to include the longitudinal current component. In this case, the numerical procedure previously depicted can be easily extended. As an example, the two strips of the studied structure are now divided into two cells along the width. Consequently, Jx basis functions are overlapped over two rows per microstrip line, until there is only one row of Jy per line. The

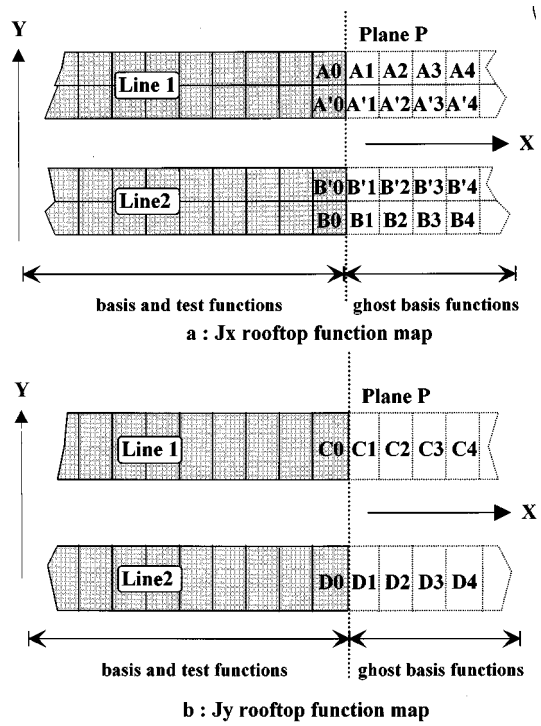

Fig. 4. Current density rooftop function map for the structure shown in Fig. 1 with a two-cell division along the strip width.

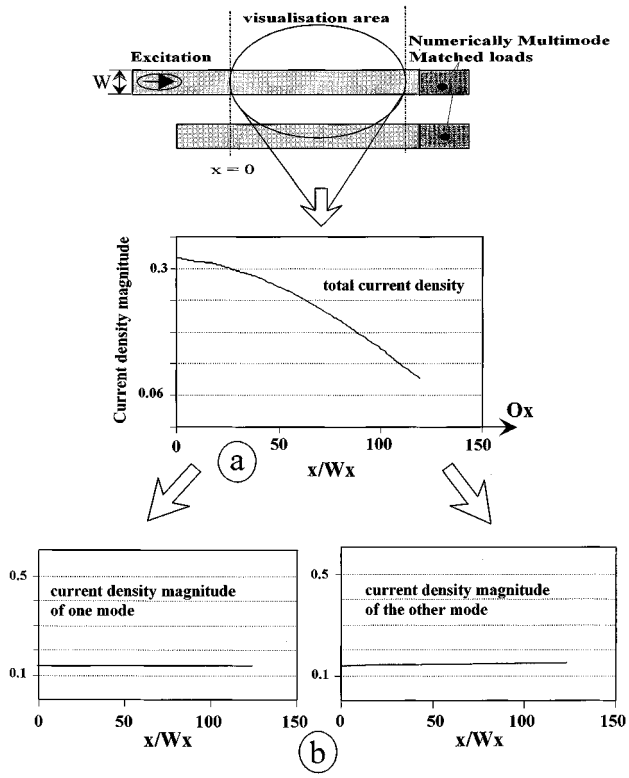

Fig. 5. Magnitude of the current density for the structure shown in Fig. 1. (a) Total current density. (b) Extracted current densities.

Jx and Jy rooftop function maps are depicted in Fig. 4. The Jx basis functions $A0$ and $B0$ are always symmetric with respect to x and it is evident that the recurrent relations (17) and (18) are always valid. The x-directed basis functions $A'0$ and $B'0$ are also symmetric with respect to x and weighting coefficients of added ghost basis functions $A'i$, $B'i$ may be related to each other with the same two coupled recurrent relations (17) and (18).

As a conclusion, when the two strips are divided over several cells along the width, each X-directed basis functions row on a line have to be associated with the X-directed basis function row on the other line with respect to the X axis symmetry. The Y-directed basis functions Jy are called Ci and Di. As shown in Fig. 4, the last Jy basis functions before the matched load are denoted $C0$ and $D0$. The weighting coefficient of these two basis functions can be expressed as

$$I_{D0} = \left(\frac{I_{C0}+I_{D0}}{2}\right) - \left(\frac{I_{C0}-I_{D0}}{2}\right) \tag{22}$$

$$I_{C0} = \left(\frac{I_{C0}+I_{D0}}{2}\right) + \left(\frac{I_{C0}-I_{D0}}{2}\right). \tag{23}$$

The Jy symmetry properties are inverse to the Jx ones, thus, $((I_{C0}-I_{D0})/2)$ and $((I_{C0}+I_{D0})/2)$ are now, respectively, the even and odd mode Jy current density amplitudes.

Equation (5) gives

$$I_{C1} = \left(\frac{I_{C0}+I_{D0}}{2}\right) \cdot e^{-2\pi j(Wx/\lambda g_o)} + \left(\frac{I_{C0}-I_{D0}}{2}\right) \cdot e^{-2\pi j(Wx/\lambda g_e)} \tag{24}$$

$$I_{D1} = \left(\frac{I_{C0}+I_{D0}}{2}\right) \cdot e^{-2\pi j(Wx/\lambda g_o)} - \left(\frac{I_{C0}-I_{D0}}{2}\right) \cdot e^{-2\pi j(Wx/\lambda g_e)}. \tag{25}$$

In these equations, the addition and subtraction of the two weighting coefficients are now associated, respectively, with the odd and even modes contrary to (6) and (7). Following a similar demonstration, weighting coefficients of added basis functions Ci, Di may be related to each other with two-coupled recurrent relation as

$$I_{Cn} = \frac{I_{C0}}{2} \cdot \left(e^{-2n\pi j(Wx/\lambda g_o)} + e^{-2n\pi j(Wx/\lambda g_e)}\right) + \frac{I_{D0}}{2} \cdot \left(e^{-2n\pi j(Wx/\lambda g_o)} - e^{-2n\pi j(Wx/\lambda g_e)}\right) \tag{26}$$

$$I_{Dn} = \frac{I_{C0}}{2} \cdot \left(e^{-2n\pi j(Wx/\lambda g_o)} - e^{-2n\pi j(Wx/\lambda g_e)}\right) + \frac{I_{D0}}{2} \cdot \left(e^{-2n\pi j(Wx/\lambda g_o)} + e^{-2n\pi j(Wx/\lambda g_e)}\right). \tag{27}$$

The weighting coefficients of the added Jy basis functions are also then related to the I_{C0}, I_{D0} unknown coefficients. As with X-directed basis functions, each Y-directed basis functions row on a line will both be associated with the symmetrical row.

In order to complete the generalization of this numerical technique, the NMML can be extended to coplanar lines. When slot or coplanar lines are taking into account, the equivalence principle allows us to describe these structures with the help

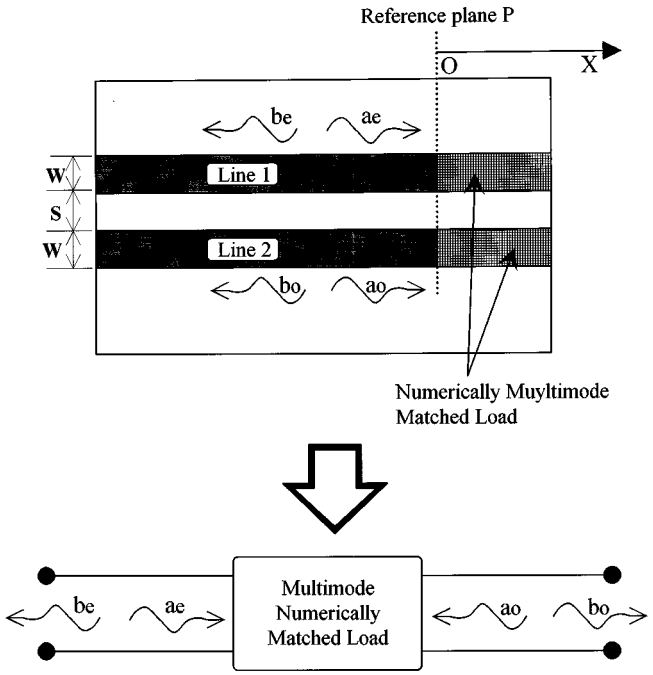

Fig. 6. Two-port model of the NMML.

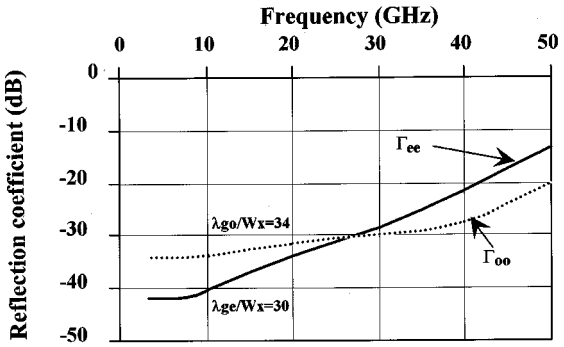

Fig. 7. Magnitude of the reflection coefficient for the NMML. The NMML has been built with five added ghost basis functions for each basis function row.

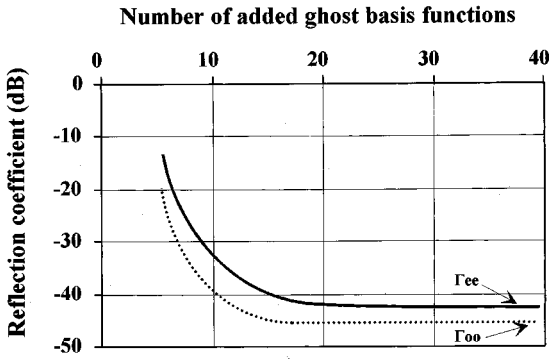

Fig. 8. Magnitude of the reflection coefficient for the NMML versus the number of added ghost basis functions. The frequency is 30 GHz.

of magnetic currents in the slots. The continuity condition of the tangential magnetic fields leads to a magnetic-field integral equation, where the magnetic field is expressed as integrals of unknown induced magnetic currents [18], [19]. Following the well-known procedure of the moment method, the equivalent magnetic current $\vec{M}_S$ on the apertures can be approximated by a set of subsectional rooftop functions $\vec{M}_X$ and $\vec{M}_Y$. Following the same procedure, an NMML can be modeled by using (17) and (18) or (26) and (27) in order to respect the symmetry properties of $\vec{M}_Y$ and $\vec{M}_X$ associated with the two modes families.

4) Numerical Results and Validating Examples: Before calculating the S-parameters of multimode waveguide discontinuities, we first check the efficiency of the NMML. With this purpose, a basic multimode structure, shown in Fig. 1, have been considered. This studied structure is composed of a microstrip-coupled line connected to an excitation microstrip line. The asymmetric discontinuity between the two waveguides guarantees us that the two modes propagate in the microstrip coupled-line waveguide. An NMML then terminates the two-coupled lines. All the microstrip lines are divided into three cells along the width of the strip. The length Wx of the half-basis functions is chosen to be about 1/13 wavelength, which is enough to represent the variations of the field satisfactorily. The NMML are built with 15 added ghost basis functions for each basis function row. As a result, each metallic strip is connected to 45 ghost basis functions. As an example, Γ_{oe} is the reflection coefficient of the odd mode due to the incident even mode of unit amplitude. (a_e, b_e) and (a_o, b_o) are, respectively, the modal amplitudes of the forward and backward even and odd modes. Γ_{eo} and Γ_{oe} have been naturally found to be equal to zero. The evolution of the magnitude of the two other reflection coefficients versus the frequency is shown in Fig. 7. In this example, the NMML has been built with five added ghost basis functions for each basis function row. As can been seen in this figure, the magnitude of the reflection coefficients increase with the frequency. If the values are acceptable for frequency lower than 10 GHz, −14 and −20 dB are not enough to impose the cancellation of the reflected waves at a frequency equal to 50 GHz. Consequently, a convergence study has been performed. In this mind, we show in Fig. 8 the magnitude of the reflection coefficients for the NMML versus the number of added ghost basis functions for each basis function row. The considered structure is always shown in Fig. 1. In this example, the frequency is equal to 50 GHz. From Fig. 8, it becomes evident that the length of the NMML is a very important parameter. Calling L this parameter, the convergence of Γ_{ee} and Γ_{oo} is, respectively, obtained for

$$L = \frac{\lambda_{ge}}{2} \quad \text{and} \quad L = \frac{\lambda_{go}}{2}. \tag{29}$$

The frequency is 10 GHz. We show in Fig. 5 the current density magnitudes of the two modes supported by the structure shown in Fig. 1. These two current densities [see Fig. 5(b)] are extracted from the total current density [see Fig. 5(a)] with the matrix pencil. As shown in Fig. 5(b), a traveling-wave configuration is obtained for the two electric surface current distributions before the NMML and validates our numerical simulation.

In a next step, the influence of the NMML length has been tested. In this mind, the matrix pencil technique is used to decompose the currents along the lines into forward- and backward-traveling waves. Using a two-port model, shown in Fig. 6,

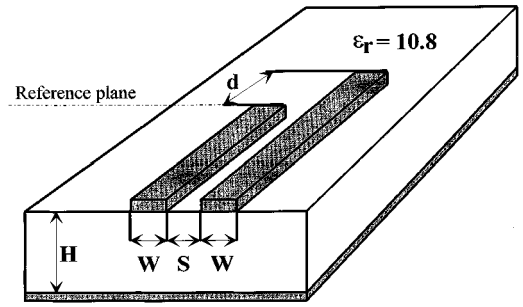

Fig. 9. Studied asymmetric microstrip coupled-line open end. $W = 500$ μm, $S = 500$ μm, $H = 635$ μm.

the NMML have been characterized by a 2×2 scattering matrix. This leads to

$$\begin{pmatrix} b_e \\ b_o \end{pmatrix} = \begin{pmatrix} \Gamma_{ee} & \Gamma_{eo} \\ \Gamma_{oe} & \Gamma_{oo} \end{pmatrix} \cdot \begin{pmatrix} a_e \\ a_o \end{pmatrix}. \tag{28}$$

Naturally, the considered value has to be the biggest one. The NMML is built with N added ghost basis functions for each basis functions row. If X represents the propagation direction, N is given by

$$N = \frac{L}{W_X} = \frac{\lambda_{g\max}}{2 \cdot W_X} \tag{30}$$

where W_X is the length of the unit rectangular cell with respect to the X-direction.

Concerning the central processing unit (CPU) time, This parameter do not suffer from the used of the NMML. In fact, the CPU time associated with the final matrix building is lower than the time used to resolve this system of equations. In greater detail, the final matrix system size and then the necessary computing time to resolve this problem is not dependent on the NMML presence because no more unknown have to be taking into account. 10 or 15 min (per frequency) on a 250 4/266 Digital Alpha Station are generally enough to obtain satisfactorily small numerical errors for the studied examples in this paper. This time is naturally depending on the device complexity (number of unknowns) and the hardware performances.

III. Application to Multimode Waveguide Discontinuities Analysis

To demonstrate the capabilities of this approach, a few results are presented in this section and compared with measured and available data.

A. First Application—Characterization of Mode Conversion in an Asymmetric Microstrip Coupled-Line Open End

The considered structure is shown in Fig. 9. The ground plane and dielectric substrate extend to infinity in the X- and Y-directions. The conductor is assumed to be perfect and of zero thickness. The surface current distributions on the coupled lines are determined by the method of moments. The matrix pencil is then used to split the currents along the lines into forward and backward multimode traveling-wave amplitudes. This is

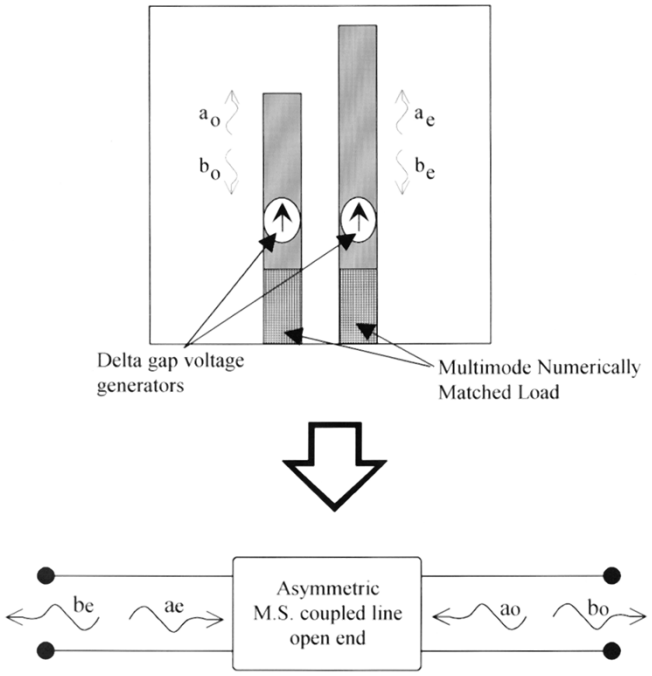

Fig. 10. Two-port model of the asymmetric microstrip coupled-line open end.

used to compute a generalized scattering matrix accounting for the propagation of two quasi-TEM modes. Using the two-port model shown in Fig. 10, mode conversion from the even to odd mode leads to a 2×2 scattering matrix between the modal amplitudes

$$\begin{pmatrix} b_e \\ b_o \end{pmatrix} = \begin{pmatrix} \Gamma_{ee} & \Gamma_{eo} \\ \Gamma_{oe} & \Gamma_{oo} \end{pmatrix} \cdot \begin{pmatrix} a_e \\ a_o \end{pmatrix}. \tag{31}$$

For example, Γ_{oe} is the reflection coefficient of the odd mode due to an incident even mode of unit amplitude, and Γ_{oo} is the reflection coefficient of the odd mode due to an incident odd mode excitation. When the scattering parameters between two modes with different field maps are calculated, e.g., Γ_{eo} and Γ_{oe}, these values are highly sensitive to the definition used to obtain the characteristic impedance. For a passive device, this difficulty can be easily overcome by using the reciprocity theorem. Thus, we do not need to normalize with respect to the even and odd characteristic impedance to obtain Γ_{eo} and Γ_{oe}. According to (31), two independent excitations are required to determine all of the elements in the scattering matrix. The NMML is placed before the delta-gap generators in order to avoid reflection waves from the excitation mechanism. The reflection coefficients of the studied structure are presented in Fig. 11. For the sake of comparison, an analytical model is also applied to analyze the mode conversion [28]. A multimode TRL calibration, presented in [20], is also used to derive experimental multimode S-parameters. Measurements were carried out at the Institut d'Electronique et de Microélectronique du Nord, Villeneuve d'Ascq, France, using a conventional vector network analyzer (VNA). Connection of multimode standards to the VNA was made using microstrip to coaxial test fixtures. More details of the TRL algorithm are given in [20].

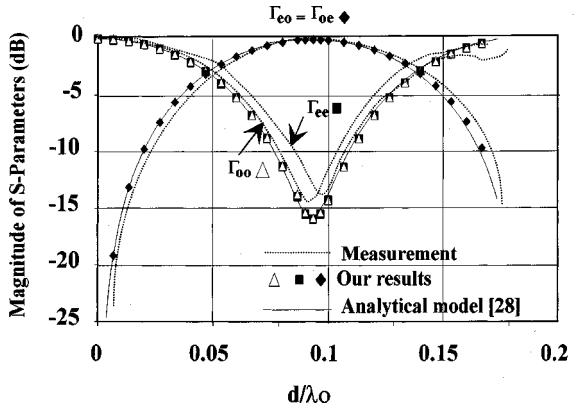

Fig. 11. Magnitude of the reflection coefficients for the asymmetric microstrip coupled-line open end shown in Fig. 9.

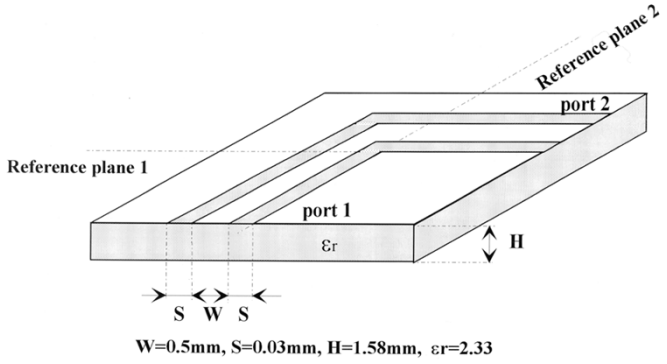

Fig. 12. Studied CPW right-angle bend.

A significant observation, shown in Fig. 11, is that Γ_{eo} and Γ_{oe} are close to 0 dB for $d/\lambda_o \approx 0.1$. This implies that when one mode is excited, all the power can be reflected back by the other mode. More detailed discussions about this mode conversion are given in [3] and [29]. As can been seen in Fig. 11, excellent agreement can be found between the results obtained with the full-wave approach, the analytical model, and the experiment ones.

B. Second Application: Mode Conversion in a CPW Right-Angle Bend

The studied CPW 90° bend discontinuity is shown in Fig. 12. The whole region of the original problem has been split into two separate ones by applying the well-known Schekunoff's equivalence principle, which introduces an equivalent magnetic current on the apertures Ms. This magnetic current along the CPW can be described by the superposition of the even coplanar mode, the odd slotline mode, and other higher order modes near the bend discontinuity. An NMML has been placed at each port of the device. Given the magnetic current distribution, the matrix pencil approach is employed to extract the propagation constants and modal amplitudes of all the guided modes. These

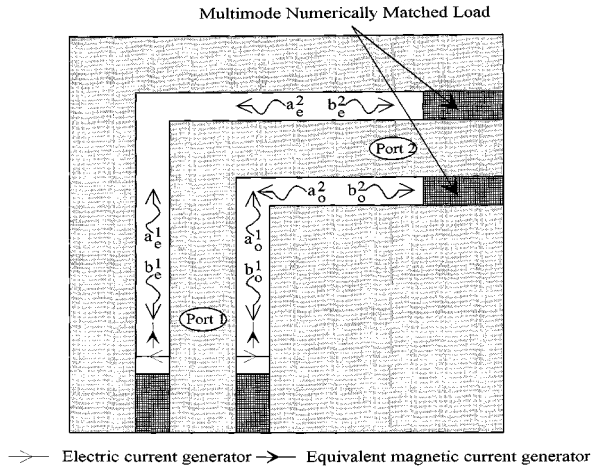

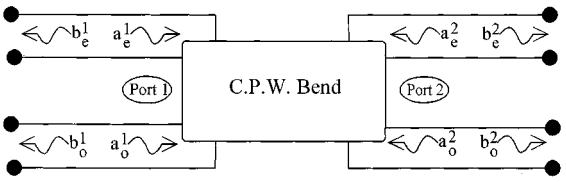

Fig. 13. Four-port model of the CPW bend.

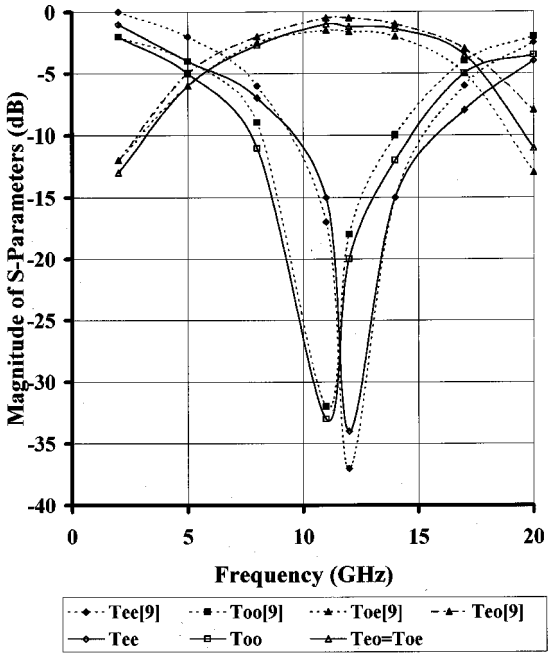

Fig. 14. Magnitude of the transmission coefficients for the CPW bend shown in Fig. 12.

modal amplitudes can be related by a 4 × 4 scattering matrix. Using the four-port model, presented in Fig. 13, this leads to

$$\begin{pmatrix} b_{1e} \\ b_{1o} \\ b_{2e} \\ b_{2o} \end{pmatrix} = \begin{pmatrix} \Gamma_{ee} & \Gamma_{eo} & T_{ee} & T_{eo} \\ \Gamma_{oe} & \Gamma_{oo} & T_{oe} & T_{oo} \\ T_{ee} & T_{eo} & \Gamma_{ee} & \Gamma_{eo} \\ T_{oe} & T_{oo} & \Gamma_{oe} & \Gamma_{oo} \end{pmatrix} \cdot \begin{pmatrix} a_{1e} \\ a_{1o} \\ a_{2e} \\ a_{2o} \end{pmatrix}. \quad (32)$$

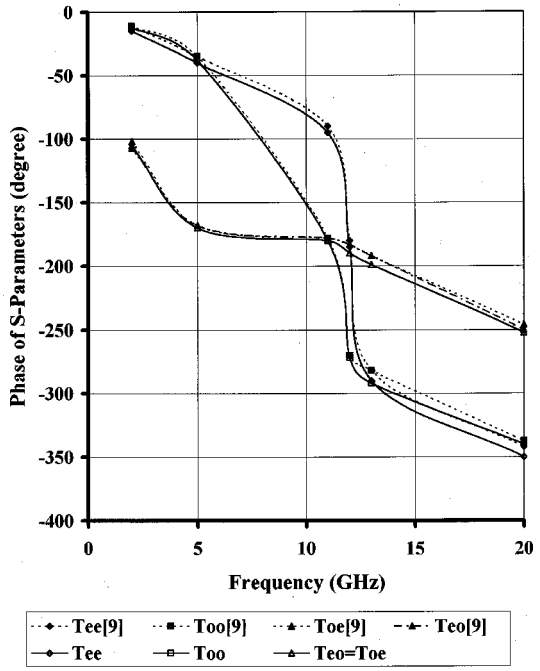

Fig. 15. Phase of the transmission coefficients for the CPW bend shown in Fig. 12.

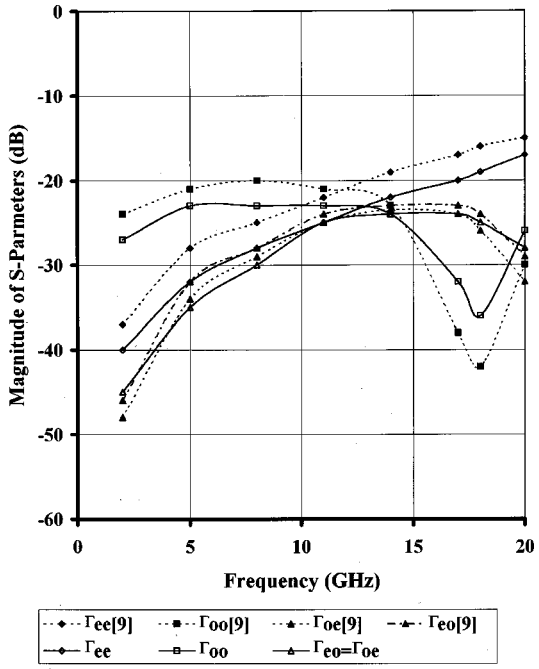

Fig. 16. Magnitude of the reflection coefficients for the CPW bend shown in Fig. 12.

As an example, a_{2o} and b_{2o} are, respectively, the incoming and outgoing modal amplitudes for the odd mode at port 2; T_{ee} is the transmission coefficient of the even mode. Due to the structure symmetry, the scattering matrix in (32) includes eight different elements, and two independent excitations will suffice to solve the desired scattering matrix. The scattering parameters between the even and odd modes are also determined with the help of the reciprocity theorem. Figs. 14 and 15 present the magnitude and phase of the transmission coefficients for the CPW

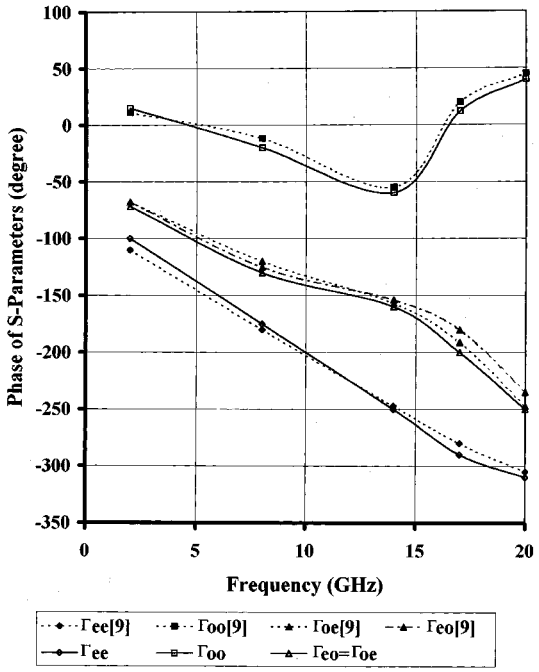

Fig. 17. Phase of the reflection coefficients for the CPW bend shown in Fig. 12.

bend shown in Fig. 12. The magnitude and phase of the reflection coefficients are shown in Figs. 16 and 17. The transmission coefficients between the even and odd modes reach the maximum while T_{ee} and T_{oo} become very small. This phenomenon occurs in the frequency range where the path difference between the outer and inner slots is close to one-half of the waveguide wavelength [9]. The magnitudes of all the transmission coefficients are seen to be very close to the referenced ones and validate our approach. A small disagreement is observed in the reflection coefficients. In general, the reflection coefficients are one order of magnitude smaller than the transmission coefficients and, consequently, they are comparatively more sensitive to numerical errors. An experiment would certainly be unable to distinguish the better result.

IV. Conclusion

In this paper, we have presented a multimode waveguide discontinuities analysis. A powerful technique is obtained by combining a spectral-domain moment method: the matrix pencil technique and an original NMML formulation. One of the advantages of the NMML lies in the fact that S-parameters may be numerically measured in the way that they are defined: that means with nonreflective generators and matched loads on each physical port. This method is fully compatible with the integral-equation technique because the reaction terms computed between each test and basis functions are sufficient to build the matched loads; no additional load current density functions are needed. Each ghost basis function coefficient is only related to that of a regular basis function; then the final matrix system does not inflate with matched loads. To demonstrate the capabilities of this approach, several examples have been presented and successfully compared to experimental measurements and

available published data. This NMML can be easily extended to waveguide analysis when more than two modes propagate.

REFERENCES

[1] M. Hirano, K. Nishikawa, I. Toyoda, S. Aoyama, S. Sugitani, and K. Yamasaki, "Three-dimensional passive circuit technology for ultra-compact MMIC's," *IEEE Trans. Microwave Theory Tech.*, vol. 43, pp. 2845–2849, Dec. 1995.

[2] I. Toyoda, T. Tokumitsu, and M. Masayoshi, "Highly integrated three-dimensional MMIC single-chip receiver and transmitter," *IEEE Trans. Microwave Theory Tech.*, vol. 44, pp. 2340–2346, Dec. 1996.

[3] J. L. Cina and L. Carin, "Mode conversion and leaky-wave excitation at open-end coupled-microstrip discontinuities," *IEEE Trans. Microwave Theory Tech.*, vol. 43, pp. 2066–2072, Sept. 1995.

[4] T. Becks and I. Wolff, "Full-wave analysis of various coplanar bends and T-junctions with respect to different types of air-bridges," in *IEEE MTT-S Int. Microwave Symp. Dig.*, Atlanta, GA, 1993, pp. 697–700.

[5] R. W. Jackson, "Mode conversion at discontinuities in finite-width conductor-backed coplanar waveguide," *IEEE Trans. Microwave Theory Tech.*, vol. 37, pp. 1582–1589, Oct. 1989.

[6] W. Heinrich, J. Gerdes, J. Heine, K. Strohm, and F. Beisswanger, "The coplanar-to-microstrip transition: Basic considerations and realization," in *MIOP'97 Conf. Proc.*, Stuttgart, Germany, pp. 370–374.

[7] K. Beilenhoff and H. L. Hartnagel, "Parasitic mode coupling at short and open circuits in coplanar MMIC's," in *MIOP'97 Conf. Proc.*, Stuttgart, Germany, pp. 408–412.

[8] N. I. Dib, M. Gupta, G. E. Ponchak, and L. P. B. Katehi, "Characterization of asymmetric coplanar waveguide discontinuities," *IEEE Trans. Microwave Theory Tech.*, vol. 41, pp. 1549–1558, Sept. 1993.

[9] M.-D. Wu, S.-M. Deng, R.-B. Wu, and P. Hsu, "Full-wave characterization of the mode conversion in a coplanar waveguide right-angled bend," *IEEE Trans. Microwave Theory Tech.*, vol. 43, pp. 2532–2538, Nov. 1995.

[10] N. H. Koster, S. Koblowski, R. Bertenburg, S. Heinen, and I. Wolff, "Investigation of air-bridges used for MMIC's in CPW technique," in *Proc. 19th European Microwave Conf.*, London, U.K., 1989, pp. 666–671.

[11] A. A. Omar and Y. L. Chow, "A solution of waveguide with air-bridges using complex images," *IEEE Trans. Microwave Theory Tech.*, vol. 40, pp. 2070–2077, Nov. 1992.

[12] ——, "Coplanar waveguide with top and bottom shields in place of air bridges," *IEEE Trans. Microwave Theory Tech.*, vol. 41, pp. 1559–1563, Sept. 1993.

[13] G. Splitt and M. Davidovitz, "Guidelines for design of electromagnetically coupled microstrip patch antennas on two-layer substrates," *IEEE Trans. Antennas Propagat.*, vol. 38, pp. 1136–1140, July 1990.

[14] T. Becks and I. Wolff, "Analysis of 3-D metallization structures by a full-wave spectral domain technique," *IEEE Trans. Microwave Theory Tech.*, vol. 40, pp. 2219–2227, Dec. 1992.

[15] Y. Hua and T. Sarkar, "Generalized pencil-of-function method for extracting poles of an EM system from its transient response," *IEEE Trans. Antennas Propagat.*, vol. 37, pp. 229–234, Feb. 1989.

[16] ——, "Matrix pencil method for estimating parameters of exponentially damped/undamped sinusoids in noise," *IEEE Trans. Acoust., Speech, Signal Processing*, vol. 38, pp. 814–824, May 1990.

[17] T. K. Sarkar, F. Hu, Y. Hua, and M. Wicks, "A real time signal processing technique for approximating a function by a sum of complex exponentials utilizing the matrix pencil approach," *Signal Process.*, vol. 4, no. 2, pp. 127–170, Apr. 1994.

[18] M. Kahrizi, T. K. Sarkar, and Z. A. Maricevic, "Analysis of a wide radiating slot in the ground plane of a microstrip line," *IEEE Trans. Microwave Theory Tech.*, vol. 41, pp. 29–36, Jan. 1993.

[19] A. B. Kouki, R. Mittra, and C. H. Chan, "Analysis of a thin slot discontinuity in the reference plane of a microstrip structure," *IEEE Trans. Microwave Theory Tech.*, vol. 41, pp. 1356–1361, Aug. 1993.

[20] C. Seguinot, P. Kennis, J. F. Legier, F. Huret, E. Paleczny, and L. Hayden, "Multimode TRL—A new concept in microwave measurements, theory and experimental verification," *IEEE Trans. Microwave Theory Tech.*, vol. 46, pp. 536–543, May 1998.

[21] G. Splitt, "A rapid method for arbitrary microstrip structure using the FFT algorithm," in *Proc. 20th European Microwave Conf.*, Budapest, Hungary, Sept. 1990, pp. 1481–1486.

[22] N. I. Dib, L. P. B. Katehi, G. E. Ponchak, and R. N. Simons, "Theoretical and experimental characterization of coplanar waveguide discontinuities for filter applications," *IEEE Trans. Microwave Theory Tech.*, vol. 39, pp. 873–881, May 1991.

[23] C. Delabie, Y. Delplanque, P. Rribetich, and P. Kennis, "Matched loads simulation using ghost basis functions for moment-method analysis: Application to microwave planar circuits," *Microwave Opt. Technol. Lett.*, vol. 7, pp. 632–637, Sept. 1994.

[24] R. Gillard, J. H. Corre, M. Drissi, and J. Citerne, "A general treatment of matched terminations using integral equations—Modeling and applications," *IEEE Trans. Microwave Theory Tech.*, vol. 42, pp. 2545–2553, Dec. 1994.

[25] P. Pannier, L. Kadri, J. F. Carpentier, F. Huret, and P. Kennis, "Efficient implementation of the numerically matched loads into the 3-D spectral domain analysis using triangular subdomain functions," *Microwave Opt. Technol. Lett.*, vol. 15, pp. 373–377, Aug. 1997.

[26] C. Delabie, "Elaboration d'un simulateur de dispositifs planaires micro-ondes. Application à la caractérization de matériaux supraconducteurs," Ph.D. dissertation, Univ. Sci. Technol., Lille, France, Sept. 1994.

[27] T. Uwaro and T. Itoh, "Spectral domain approach," in *Numerical Techniques for Microwave and Millimeter-Wave Passive Structures*, T. Itoh, Ed. New York: Wiley, 1989, pp. 334–380.

[28] P. Pannier, J. F. Carpentier, C. Seguinot, F. Huret, and P. Kennis, "Analytical and full-wave characterization of multimode waveguide discontinuities," in *Proc. 27th European Microwave Conf.*, Jerusalem, Israel, 1997, pp. 1142–1147.

[29] P. Pannier, E. Paleczny, P. Kennis, and F. Huret, "Mode conversion at discontinuities in a microstrip coupled line waveguide," *Microwave Opt. Technol. Lett.*, vol. 17, pp. 40–43, Jan. 1998.

Philippe Pannier was born in Bruay en Artois, France, on July 6, 1969. He received the Ph.D. degree from the University of Lille, Lille, France, in 1997.

From 1994 to 1997, he was involved with electromagnetics at the Institut d'Electronique et de Microélectronique du Nord. In November 1997, he joined the Laboratoire de Modélization et de Microélectronique de Marseille, Marseille, France, where he is currently an Assistant Professor. His research interests are printed antennas and design for RF integrated-circuit (RFIC) applications.

Lhoussain Kadri, photograph and biography not available at the time of publication.

Christophe Seguinot received the Ph.D. degree in electronics from the University of Lille, Lille, France, in 1988.

In 1981, he joined the Institut d'Electronique et de Microélectronique du Nord, Villeneuve d'Ascq, France, where he is currently an Assistant Professor. His work has included the characterization and modeling of microwave transmission lines and waveguides laid on semiconducting substrates. His current research is concerned with high-frequency discontinuities and interconnect simulation. In addition, he is interested in digital and mobile communications.

Patrick Kennis, photograph and biography not available at the time of publication.

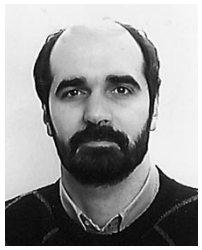

Fabrice Huret received the Ph.D. degree from the University of Lille, Lille, France, in 1991.

He is currently an Assistant Professor at the Université du Littoral–Côte d'Opale, IUT du Littoral, Calais, France. His current research interests at the Institut d'Electronique et de Microélectronique du Nord, Villeneuve d'Ascq, France, are 3-D modelization of VLSI and MMIC interconnects. His is also an Associate Member of the Laboratoire d'Etude des Matériaux et des Composants pour l'Electronique, Université du Littoral–Côte d'Opale, where his research interests are new substrate materials built with liquid crystals and applications of these materials as electrically tunable substrate RF and microwave frequency components.